Journal of Energy Storage 136 (2025) 118450

Contents lists available at ScienceDirect

Journal of Energy Storage

journal homepage: www.elsevier.com/locate/est

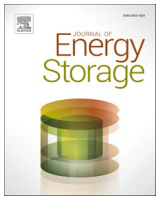

Research Papers

Data-driven evidence for the burst effect in MgH_2 dehydrogenation via analysis of experimental kinetic curves

Jianghao Cai [a,b], Haobo Wang [a,b], Xiaotian Tang [a,b], Ziwei Miao [a,b], Tongao Yao [a,b], Yuxuan Liu [a,b], Hongtao Wang [a,b], Zhengyang Gao [a,b], Weijie Yang [a,b,*]

[a] Hebei Key Laboratory of Energy Storage Technology and Integrated Energy Utilization, North China Electric Power University, Baoding, 071003, Hebei, China
[b] Department of Power Engineering, School of Energy, Power and Mechanical Engineering, North China Electric Power University, Baoding, 071003, Hebei, China

ARTICLE INFO

Keywords:
Magnesium hydride
Burst effect
Dynamic modeling
Activation energy
JMAK model
Data-driven analysis

ABSTRACT

The dehydrogenation of magnesium hydride is widely believed to involve the burst effect, in which surface hydrogen atoms rapidly desorb during the early stage, followed by a diffusion-controlled release from the bulk. However, direct kinetic evidence validating this two-stage mechanism remains limited, hindering its integration into practical hydrogen storage design. To address this gap, the present study proposes a data-driven dynamic modeling strategy based on extensive experimental data. Within a modified Johnson-Mehl-Avrami-Kolmogorov (JMAK) framework, both segment-based and continuously evolving activation energy models are established. By analyzing a large number of dehydrogenation kinetic curves collected from published literature, the dynamic evolution of kinetic parameters is quantitatively reconstructed, thereby providing solid evidence for the burst effect. The results demonstrate a sharp decline in activation energy during the initial 10 % to 20 % of the reaction, followed by stabilization in the 10 % to 90 % percent range. This trend is consistently observed across diverse datasets, reinforcing the statistical validity of the burst feature. Furthermore, a comparative analysis is conducted using average and median activation energy values from three distinct sources: theoretical calculations, experimental fittings, and dynamic model reconstructions. It is found that the initial activation energy obtained from the continuously evolving kinetic profile closely corresponds to theoretical results, while the equilibrium activation energy agrees well with experimental values. This dual correspondence reveals the physical origin of discrepancies between simulation and experiment. Overall, this work provides a data-driven framework that not only confirms the burst effect with robust experimental support but also facilitates the unified understanding of dehydrogenation kinetics in solid-state hydrogen storage systems.

1. Introduction

Under the global pursuit of sustainable and efficient energy solutions, hydrogen energy has gained increasing attention due to its high gravimetric energy density, long-term availability, and potential to decarbonize multiple sectors [1,2]. For large-scale deployment, the development of safe, cost-effective, and compact hydrogen storage technologies remains a critical challenge. Common strategies include high-pressure gaseous storage [3], cryogenic liquid storage [4], and solid-state storage [5]. Among these, solid-state hydrogen storage based on metal hydrides offers a promising balance between storage capacity, safety, and system integration potential, making it particularly suitable for stationary and mobile energy storage systems [6]. Among metal hydrides, magnesium-based hydrogen storage materials are of particular interest due to their high theoretical hydrogen capacity, low raw material cost, and natural abundance [7,8]. These characteristics make them attractive candidates for integration into renewable energy storage systems, portable hydrogen supply modules, and hybrid power devices. However, the practical use of magnesium-based materials is significantly hindered by their inherently slow hydrogen absorption and desorption kinetics, especially under moderate temperatures and pressures [9]. These kinetic limitations are particularly pronounced during the dehydrogenation process [10–12]. The release of hydrogen from MgH_2 involves complex and rate-limiting steps, such as nucleation of the Mg phase, growth of the Mg/MgH_2 interface, and solid-state hydrogen diffusion [13–15]. Furthermore, strong Mg—H bonding results in high

* Corresponding author at: Hebei Key Laboratory of Energy Storage Technology and Integrated Energy Utilization, North China Electric Power University, Baoding, 071003, Hebei, China.
E-mail address: yangwj@ncepu.edu.cn (W. Yang).

https://doi.org/10.1016/j.est.2025.118450
Received 26 June 2025; Received in revised form 13 August 2025; Accepted 14 September 2025
Available online 20 September 2025

activation energies, while surface passivation and limited catalytic activity further suppress the reaction rate [16].

To address this challenge, considerable efforts have been devoted to elucidating the dehydrogenation mechanisms of magnesium-based systems. Various classical kinetic models have been proposed to interpret the isothermal dehydrogenation behavior and to uncover the correlations between observed reaction rates and the underlying physical or chemical transformations [17]. Among them, the contracting volume model assumes that the reaction proceeds inward from the particle surface and is controlled by either interfacial reaction or diffusion, making it suitable for systems with regular particle morphology [18,19]. Diffusion-controlled models, including 1-D, 2-D and 3-D frameworks, consider hydrogen diffusion through the product layer as the rate-limiting step and are commonly used to analyze the diffusion-restricted stage in the latter part of the reaction [20]. The Prout-Tompkins model incorporates autocatalytic effects to describe systems where the reaction rate accelerates with conversion, especially during self-accelerating reaction phases [21]. In addition to these models, researchers have also employed iso-conversional methods under isothermal conditions, such as the Friedman method and other model-free techniques, to extract kinetic parameters. However, these approaches mainly focus on data fitting and lack physical modeling of the reaction mechanism [22,23]. Among the various kinetic models, the Johnson-Mehl-Avrami-Kolmogorov (JMAK) model has been widely adopted due to its physical significance in describing nucleation and growth mechanisms during dehydrogenation of magnesium-based materials [24–26]. In recent studies, several extensions of the JMAK model have been developed, including variable nucleation rates, non-uniform grain distributions, particle size effects and interfacial resistance, in order to enhance its applicability [27–30]. However, the conventional JMAK model yields fixed kinetic parameters, which limits its ability to reveal the intrinsic dynamic characteristics of the dehydrogenation process in magnesium-based hydrogen storage materials.

Kapischke et al. were the first to apply a temperature oscillation technique in a non-permeable packed bed of fine-grained material and observed that the effective thermal conductivity of MgH_2 varied with temperature, with related thermophysical quantities such as thermal diffusivity and specific heat capacity taken into account in their analysis [31]. Zhou et al. investigated the growth behavior of metallic magnesium during the dehydrogenation of MgH_2 nanoparticles and revealed a distinct transitional mechanism [32]. The growth of Mg microcrystals was divided into three stages, with a slow dehydrogenation rate in the first stage followed by a significant acceleration in the second. Karst et al. employed a self-supporting membrane for in situ nanoscale imaging to uncover the kinetic details of the transformation from metallic Mg to dielectric MgH_2 at the nanoscale [33]. Phonon resonance in MgH_2 was shown to provide unprecedented chemical specificity between different states of matter. Their results demonstrated that the hydride phase nucleates at grain boundaries and then propagates into neighboring nanocrystals, further revealing the dynamic nature of MgH_2 kinetic evolution. In our previous work [34], we systematically investigated the layer-by-layer dehydrogenation mechanism of MgH_2 using density functional theory and ab initio molecular dynamics simulations. Through this study, we first proposed and defined the concept of the “burst effect”, referring to the phenomenon in which the energy barrier for the initial surface hydrogen desorption is markedly higher than that for the subsequent hydrogen migration and desorption steps. As the surface becomes partially dehydrogenated, the Mg—H bonds weaken and the activation energy decreases sharply before stabilizing, leading to a clear transition from sluggish to accelerated dehydrogenation. Based on this newly identified burst effect, we further established the first kinetic prediction model for solid-state hydrogen storage systems [35]. The burst effect highlights the intrinsic dynamic evolution during the dehydrogenation of magnesium-based materials, providing both mechanistic insight and predictive capability for their hydrogen storage performance. However, existing macroscopic kinetic models fail to adequately capture this trend. Therefore, there is an urgent need for a modeling approach capable of continuously describing the evolution of kinetic parameters in order to validate the effectiveness of the burst effect at the macroscopic scale. In pyrolysis studies, the Distributed Activation Energy Model (DAEM) has been widely adopted to characterize the complex kinetics of multistep reactions [36,37]. This approach treats the overall reaction as a superposition of numerous elementary reactions with different activation energies. By constructing a probability density function of activation energy, DAEM enables statistical fitting of diverse reaction pathways and reveals the continuous variation of kinetic barriers over the course of the reaction [38–40].

Inspired by this methodology, the present study introduces a data-driven modeling framework to construct a continuously evolving kinetic profile based on a large number of isothermal dehydrogenation datasets. To systematically investigate the kinetic evolution of magnesium hydride during hydrogen release, the framework extends the classical JMAK model by integrating both segment-based and continuous strategies. A comprehensive set of experimental reaction curves is statistically analyzed to reverse-fit the apparent activation energy as a function of reaction progress. The resulting profiles consistently demonstrate an initial rapid decline in activation energy, followed by a stable plateau, which closely aligns with the burst effect observed in theoretical simulations. A quantitative comparison of the activation energies in early and stabilized stages reveals a difference range that corresponds well with the reported discrepancy between theoretical predictions and experimental fittings. This dynamic profile, constructed from large-scale datasets and validated through model-driven analysis, offers strong multiscale evidence for the burst effect and contributes to resolving the long-standing disagreement between simulation and experiment. Furthermore, by eliminating artificial discontinuities and enhancing the physical interpretability of kinetic parameters, the proposed modeling framework presents a more accurate and application-relevant tool for analyzing solid-state hydrogen storage systems.

2. Model construction and method

To characterize the kinetic evolution of the dehydrogenation process in magnesium hydride, this work establishes a data-driven modeling framework by extending the classical JMAK model [6]. Originally developed to describe phase transformations in solid-state materials, the JMAK model has been widely adopted in the study of solid-state hydrogen storage systems due to its ability to capture nucleation and growth mechanisms under isothermal conditions [41–43]. In the context of magnesium-based hydrides, the model provides a flexible yet physically interpretable means of describing the apparent reaction rate as a function of time and conversion. The proposed framework further expands the classical formulation by allowing both the activation energy and the Avrami exponent to evolve continuously with the reaction progress. This enhancement enables the model to reflect time-dependent changes in the dominant rate-limiting steps, including surface desorption and bulk diffusion. As a result, the framework is capable of capturing dynamic kinetic features such as the burst effect, thereby offering a more comprehensive and application-relevant interpretation of dehydrogenation behavior in solid-state hydrogen storage materials.

The modeling procedure involves two main steps. First, a segment-based fitting strategy is implemented to extract apparent kinetic parameters at different conversion levels. Each isothermal dehydrogenation curve is divided into multiple equal-conversion intervals, and every segment is independently fitted using the JMAK equation to obtain discrete values of activation energy and Avrami exponent. This method ensures high local fitting accuracy while accommodating the kinetic heterogeneity observed during the reaction. Subsequently, the initially extracted parameters are further optimized by iterative minimization of an error function, which effectively reduces the discrepancies arising from data acquisition and fitting, thereby ensuring more reliable kinetic profiles.

Second, continuous activation energy and Avrami exponent profiles are constructed through polynomial interpolation of the discrete results. This step eliminates non-physical discontinuities and guarantees smooth transitions between stages. The resulting continuous kinetic profiles provide a coherent representation of the reaction process, allowing for direct observation of kinetic transitions across the entire conversion range. To enable systematic comparison, three categories of kinetic parameters are defined according to their derivation strategies. These include the Conventional Kinetic Parameters (CKP), which are obtained by fitting the entire dehydrogenation curve with a single parameter set; the Segment-Based Kinetic Parameters (SBKP), which result from piecewise fitting of the curve within discrete reaction intervals; and the Continuously Evolving Kinetic Parameters (CEKP), which are generated by interpolating the segment-wise results into smooth functions of reaction progress and temperature.

This modeling approach offers a quantitative tool for detecting non-uniform behaviors, such as the rapid release of hydrogen in the early stage followed by a stabilized regime under bulk diffusion control. It reveals the temporal evolution of underlying mechanisms and provides robust evidence for the existence of the burst effect. A schematic overview of the modeling procedure is presented in Fig. 1, and detailed mathematical formulations, implementation details, and parameter settings are available in the Supporting information [44–49].

3. Results and discussion

3.1. Modeling results based on segment-based kinetic parameters (SBKP)

To systematically evaluate the applicability of the segment-based kinetic model, a large number of experimental datasets on the dehydrogenation kinetics of MgH_2, published between 2012 and 2025, were analyzed using a JMAK-guided fitting strategy. The extracted kinetic parameters were subsequently refined through error minimization procedures to enhance the accuracy of the model. Detailed results for all datasets are provided in the Supporting Information (Figs. S1–S18, Tables S1–S19). In addition, comprehensive information on the MgH_2 systems used for modeling, including synthesis methods, material purity, morphology, and reaction conditions, is summarized in Table S21 of the Supporting Information. In the main text, six representative datasets were selected for in-depth analysis due to their typical reaction characteristics and the availability of measurements at multiple temperatures, as shown in Fig. 2 [50–55]. Fig. 2(a1)–(f1) presents comparisons between experimental data and the Conventional Kinetic Parameter (CKP) model, while Fig. 2(a2)–(f2) displays the results obtained using the Segment-Based Kinetic Parameter (SBKP) model. Although the CKP approach yields reasonable agreement in the mid-reaction region, significant deviations appear at the initial and final stages. These discrepancies arise because conventional methods

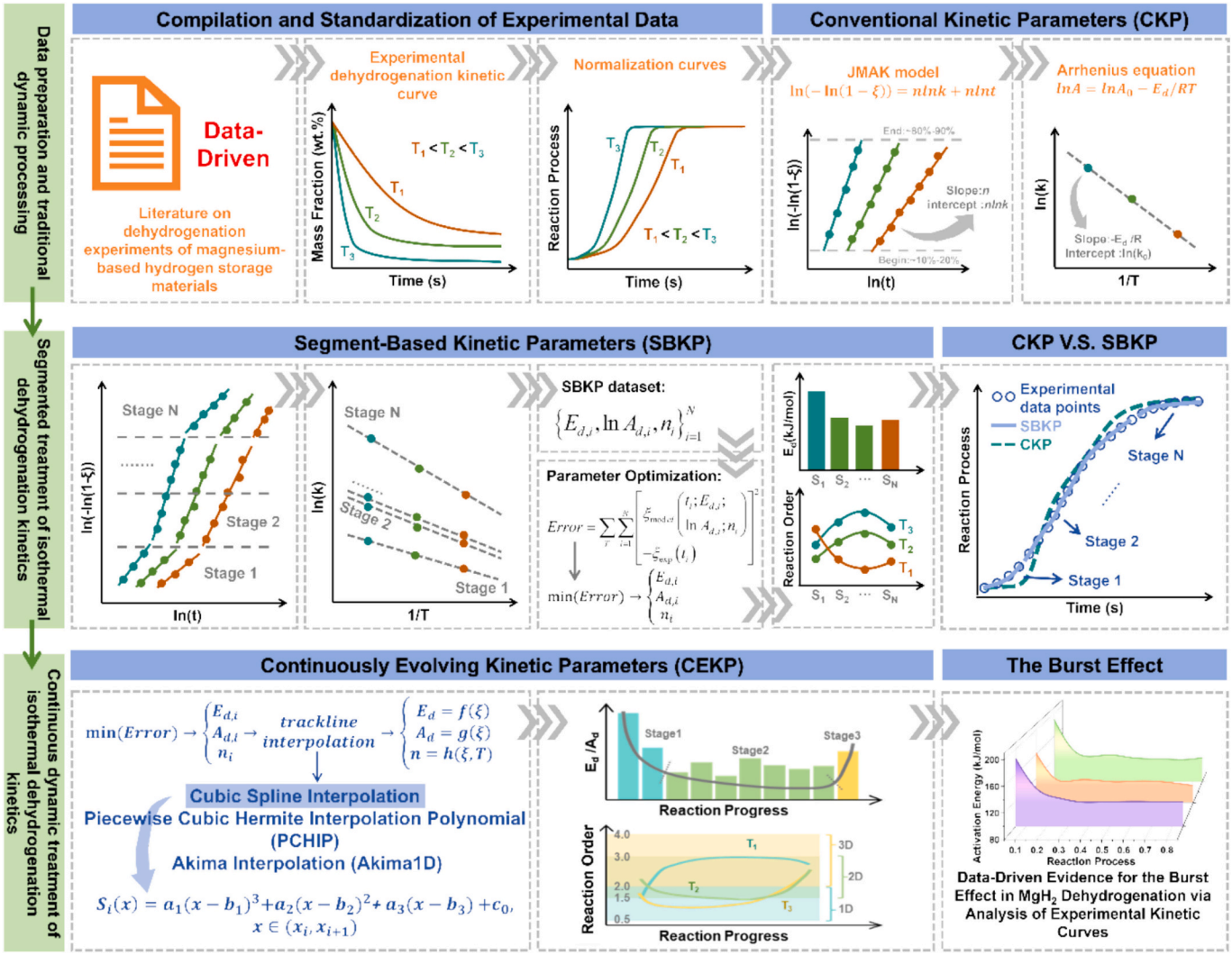

Fig. 1. Data-driven reconstruction of dehydrogenation kinetics in Mg-based hydrogen storage materials: A JMAK-Guided workflow from segment-based kinetic parameters to continuously evolving kinetic parameters.

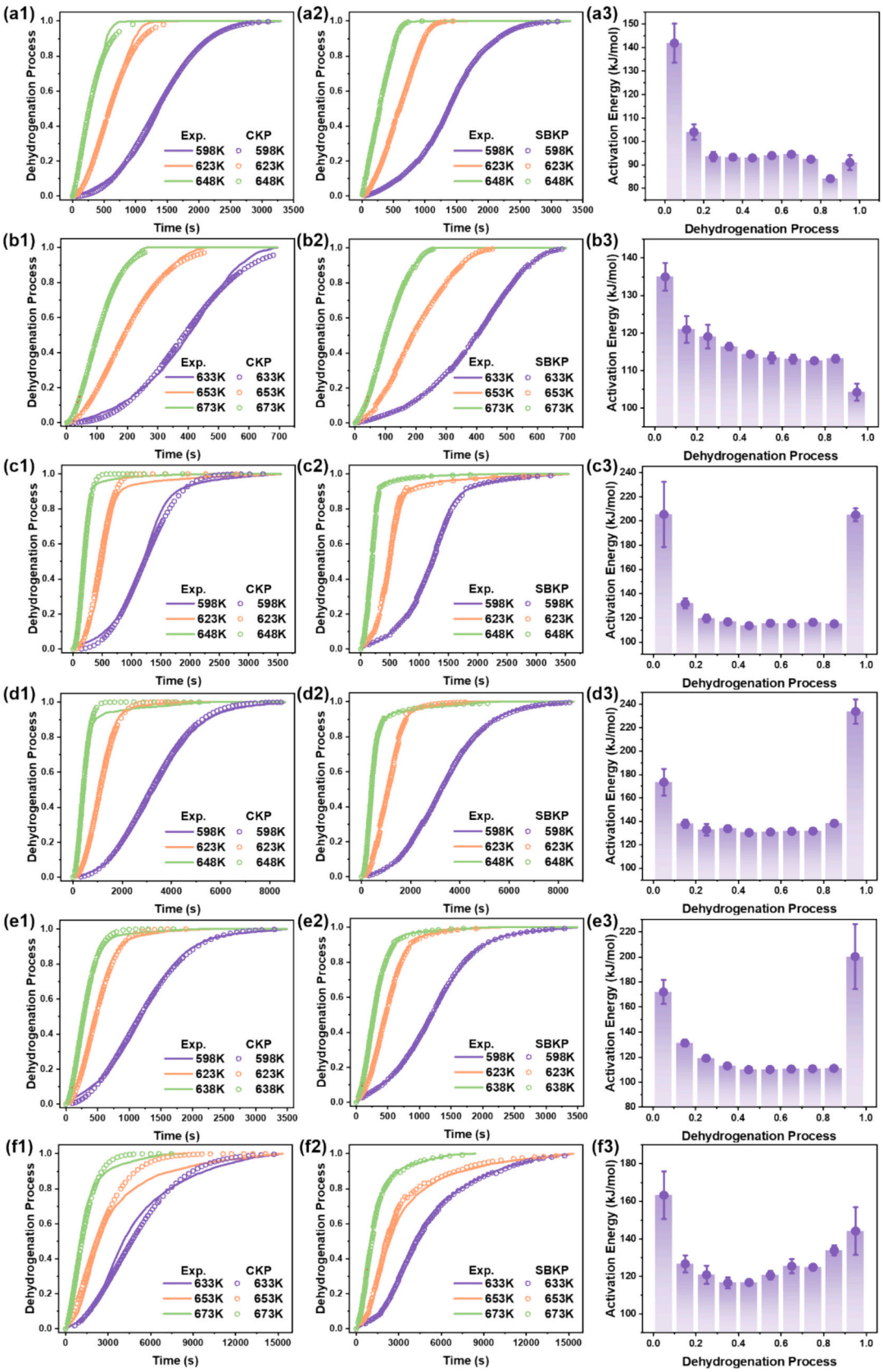

Fig. 2. Comparison of experimental measurements and kinetic modeling results for representative pure magnesium hydride systems with varying material properties [50–55]: (a1–f1) The CKP modeling results; (a2–f2) the SBKP modeling results; (a3–f3) the segment-based dehydrogenation activation energy.

typically derive kinetic parameters from the stable portion of the curve, thereby neglecting nucleation and desorption phases. In contrast, the SBKP model substantially improves fitting accuracy across the full reaction span. This improvement is further validated by the correlation coefficients from reverse fitting, summarized in Table 1, which highlight the enhanced robustness and physical relevance of the segment-based framework.

Fig. 2(a3)–(f3) shows the computed activation energy profiles derived from the Segment-Based Kinetic Parameter (SBKP) model. A clear and consistent trend is observed: during the first 90 % of the dehydrogenation process, the activation energy gradually decreases and then stabilizes. This dynamic pattern provides solid evidence in support of the burst effect mechanism previously proposed through theoretical investigations [34]. Theoretically, this behavior aligns with the understanding that dehydrogenation is initially limited by hydrogen release at grain boundaries, where kinetic barriers are highest [56]. As the surface hydrogen is consumed, hydrogen atoms from deeper regions migrate toward the Mg/MgH_2 interface and desorb more easily, resulting in a progressive decline in the apparent energy barrier and the emergence of a more uniform reaction profile. Pure MgH_2 serves as a typical system in which this kinetic feature is prominently observed. In addition, experimental dehydrogenation curves from catalyst- and alloy-modified MgH_2 samples (Table S20) were examined. Their activation energy profiles display the same initial decline followed by stabilization, further reinforcing the generality of the burst effect across different material systems.

In the final stage of the reaction, metallic magnesium gradually accumulates as the dominant phase due to the progressive conversion of MgH_2. This behavior is believed to result from the inward propagation of the reaction front: dehydrogenation preferentially initiates at grain boundaries and other high-defect regions, and gradually progresses toward the core of the particles. As the remaining MgH_2 becomes increasingly isolated and surrounded by metallic Mg, the effective reaction interface is significantly reduced. Together with the gradual depletion of hydrogen content, this results in increased resistance to dehydrogenation and a slight rebound in the apparent activation energy. As shown in Figs. S1–S6, the reaction order typically rises from the early to middle stages and then decreases toward the end of the process. This trend may indicate a mechanistic transition from one-dimensional to two-dimensional and subsequently back to one-dimensional transport behavior [32]. However, this interpretation remains hypothetical, as direct microstructural observations are currently lacking. The observed rebound in activation energy may also be partially attributed to experimental noise or limitations in the segment-based fitting methodology. Further validation using integrated theoretical simulations and real-time experimental measurements is necessary to confirm this dynamic trend. Despite these uncertainties, the Segment-Based Kinetic Parameters model effectively improves the overall fitting accuracy and reveals key mechanistic features underlying the dehydrogenation behavior. Nevertheless, the discrete nature of the model introduces non-physical discontinuities between adjacent segments, thereby limiting its ability to represent the smooth evolution of kinetic parameters across the full reaction course.

Table 1
Comparison of correlation coefficients between experimental data and CKP or SBKP modeling results.

Material	CKP modeling R^2			SBKP modeling R^2			Ref.
	T_1	T_2	T_3	T_1	T_2	T_3	
Pure MgH_2	0.996	0.992	0.989	1.000	0.999	0.999	[50]
	0.994	0.999	0.999	1.000	0.999	0.999	[51]
	0.982	0.937	0.992	0.994	0.970	0.987	[52]
	0.993	0.979	0.993	0.998	0.990	0.997	[53]
	0.995	0.994	0.998	1.000	0.998	0.999	[54]
	0.969	0.958	0.976	0.996	0.980	0.993	[55]

3.2. Evolution trends of the continuously evolving kinetic parameters (CEKP)

To ensure a continuous and physically meaningful representation of dehydrogenation kinetics in MgH_2, we developed a Continuously Evolving Kinetic Parameters (CEKP) framework. Unlike stage-based models that treat kinetic parameters as piecewise constants, the CEKP approach captures their gradual evolution across the entire reaction process through smooth interpolated functions. These functions were incorporated into the JMAK model to produce continuous reaction curves that more closely reflect the intrinsic dynamics of dehydrogenation. This methodology eliminates artificial discontinuities at segment boundaries and enhances physical interpretability by approximating the continuous evolution of kinetic parameters induced by gradual structural and compositional changes during the reaction. Although the CEKP model provides smooth and continuous functions for activation energy, pre-exponential factor, and reaction order, its reconstructed $\xi(t)$ curves show slightly lower pointwise accuracy than those obtained using SBKP. However, the main objective of the CEKP framework is not to maximize fitting precision at every point, but to recover a continuous and interpretable trend that reflects the dynamic nature of the kinetic process. Therefore, the model's validity is primarily evaluated through its alignment with known physical features and its ability to generalize across datasets.

To validate the physical basis and general applicability of the CEKP framework, a comprehensive statistical analysis was conducted using experimental kinetic data of pure MgH_2 dehydrogenation reported from 2012 to 2025 [50–55,57–79]. These datasets cover a wide range of conditions, including different synthesis methods of MgH_2, various reaction temperatures, and distinct experimental environments. Such differences in sample preparation, testing setups, and operating parameters can lead to noticeable variations in the absolute values and initial peak heights of the activation energy profiles. Despite these variations, the reconstructed activation energy profiles consistently exhibit a distinct pattern: a steep decline during the initial 10 % to 20 % of the reaction, followed by a stable plateau extending up to 90 % conversion. This trend provides strong empirical evidence for the burst effect mechanism, which was originally proposed based on first-principles calculations. It reflects the preferential release of hydrogen from high-energy grain boundary regions at the early stage, which reduces the activation barrier for subsequent desorption. The persistence of this declining-then-stabilizing pattern across all datasets confirms that these variations in initial values do not alter the underlying kinetic evolution, offering compelling support for the validity of the CEKP framework. The final 10 % of the reaction, often influenced by noise or mass transport limitations, was excluded from comparative analysis. A summary of these activation energy profiles is presented in Fig. 3(a), demonstrating the data-driven foundation and physical interpretability of the proposed model.

Inspired by the distributed activation energy model (DAEM) originally applied in pyrolysis studies [43–47], the statistical characteristics of the activation energy profiles collected from the literature were further analyzed. Although DAEM describes how reaction behavior evolves as a function of temperature under non-isothermal conditions, the present study focuses on isothermal reactions and analyzes how activation energy changes along the reaction progress. Specifically, all dynamic activation energy values derived from CEKP analysis were compiled across a wide range of MgH_2 datasets and fitted using probability density functions. As illustrated in Fig. 3(b), these data exhibit a clear unimodal distribution with a pronounced Gaussian-like shape. The peak of the distribution aligns closely with the stable region of the activation energy curve, corresponding to the 10 % to 90 % conversion interval in the CEKP model. This approach shares a similar statistical philosophy with DAEM but applies it in a different context, where the reaction coordinate is conversion rather than temperature. This consistency suggests that the majority of kinetic behavior is dominated by a

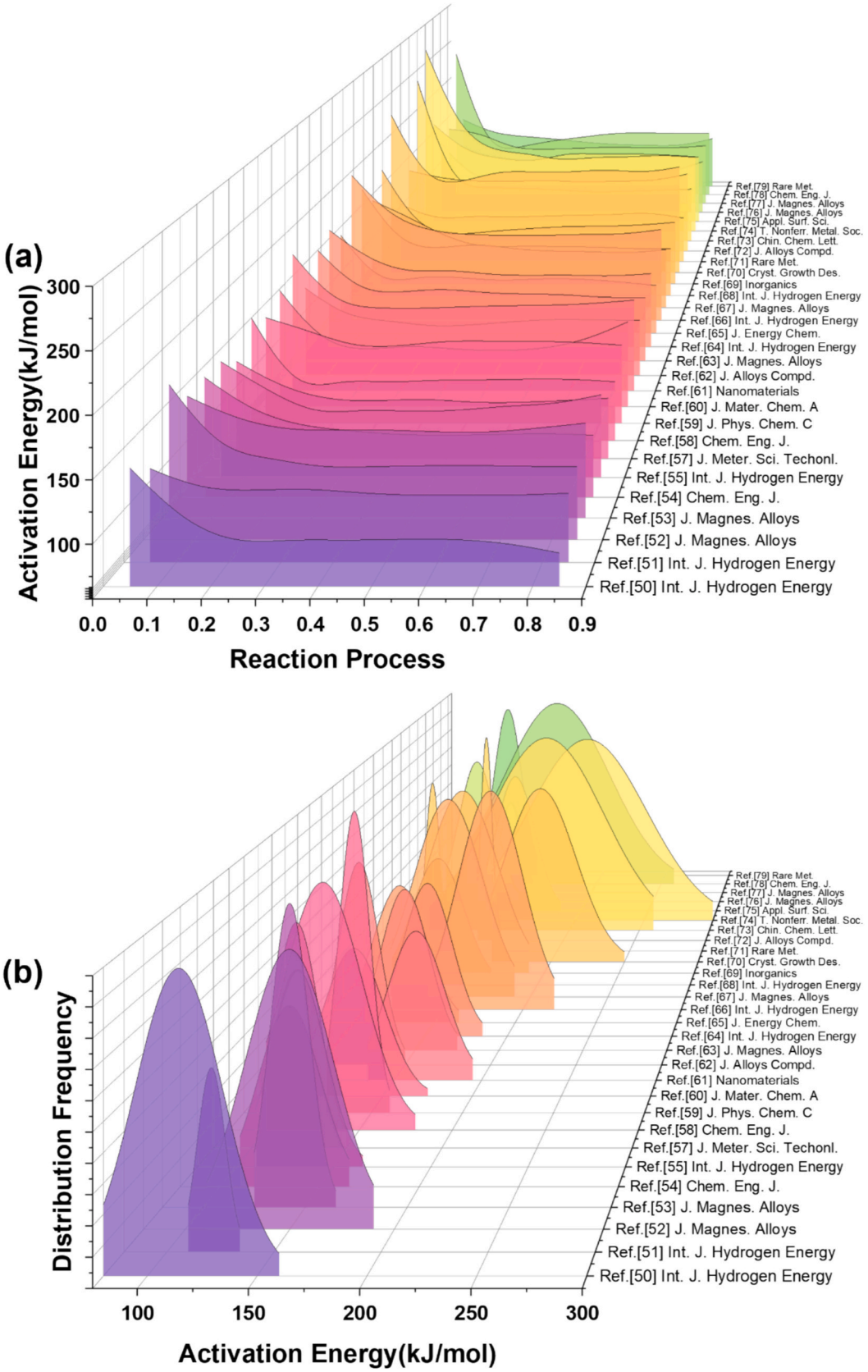

Fig. 3. Activation energy analysis based on CEKP modeling. (a) Evolution profiles during the first 90 % of pure MgH_2 dehydrogenation. (b) Probability distribution of interpolated activation energy values.

relatively narrow range of activation energies associated with bulk hydrogen migration and desorption processes. In contrast, activation energies extracted from the initial and final stages of the dehydrogenation reaction are comparatively sparse and exhibit greater variance, reflecting their susceptibility to experimental fluctuations and localized reaction conditions.

The observed normal distribution reinforces the physical credibility of the CEKP framework, as it confirms that dynamic interpolation between adjacent stages produces smooth, continuous energy profiles that are statistically centered around the most representative kinetic regime. Moreover, the statistical symmetry and central tendency of this distribution provide quantitative support for the burst effect mechanism, indicating that the high-energy barrier at the early stage is transient and followed by a kinetically favorable plateau [6]. This finding reflects a transition from localized surface-driven reactions to diffusion-controlled bulk processes, and is in excellent agreement with theoretical predictions [31–35]. Together, these insights offer a unified understanding of the entire dehydrogenation pathway in MgH_2, bridging atomic-scale models and macroscopic kinetic observations with strong experimental support.

3.3. Difference analysis between theoretical calculation and experimental fitting

After establishing the continuous activation energy model for the dehydrogenation of magnesium hydride, a significant gap was observed between the peak value and the stabilized value along the entire activation energy profile. Currently, there are two primary approaches for determining the activation energy of magnesium hydride dehydrogenation. One is based on first-principles calculations using density functional theory at the atomic scale, referred to as theoretical calculation [8,80–87]. The other relies on mathematical fitting of experimental dehydrogenation kinetics curves, referred to as experimental fitting [59,61,64,66,68–78]. To better understand the origin of this discrepancy, we compiled representative activation energy values reported in the literature using both methods. For theoretical calculations, we selected only studies focused on pure MgH_2 systems without catalytic modification, and specifically those that reported activation barriers for surface hydrogen desorption processes. These values typically correspond to the formation of the first hydrogen vacancies and represent the most energetically demanding steps at the early stage of dehydrogenation. The reported values were obtained under idealized modeling conditions, such as slab geometries with defined crystallographic surfaces and limited hydrogen coverage. Therefore, they are particularly

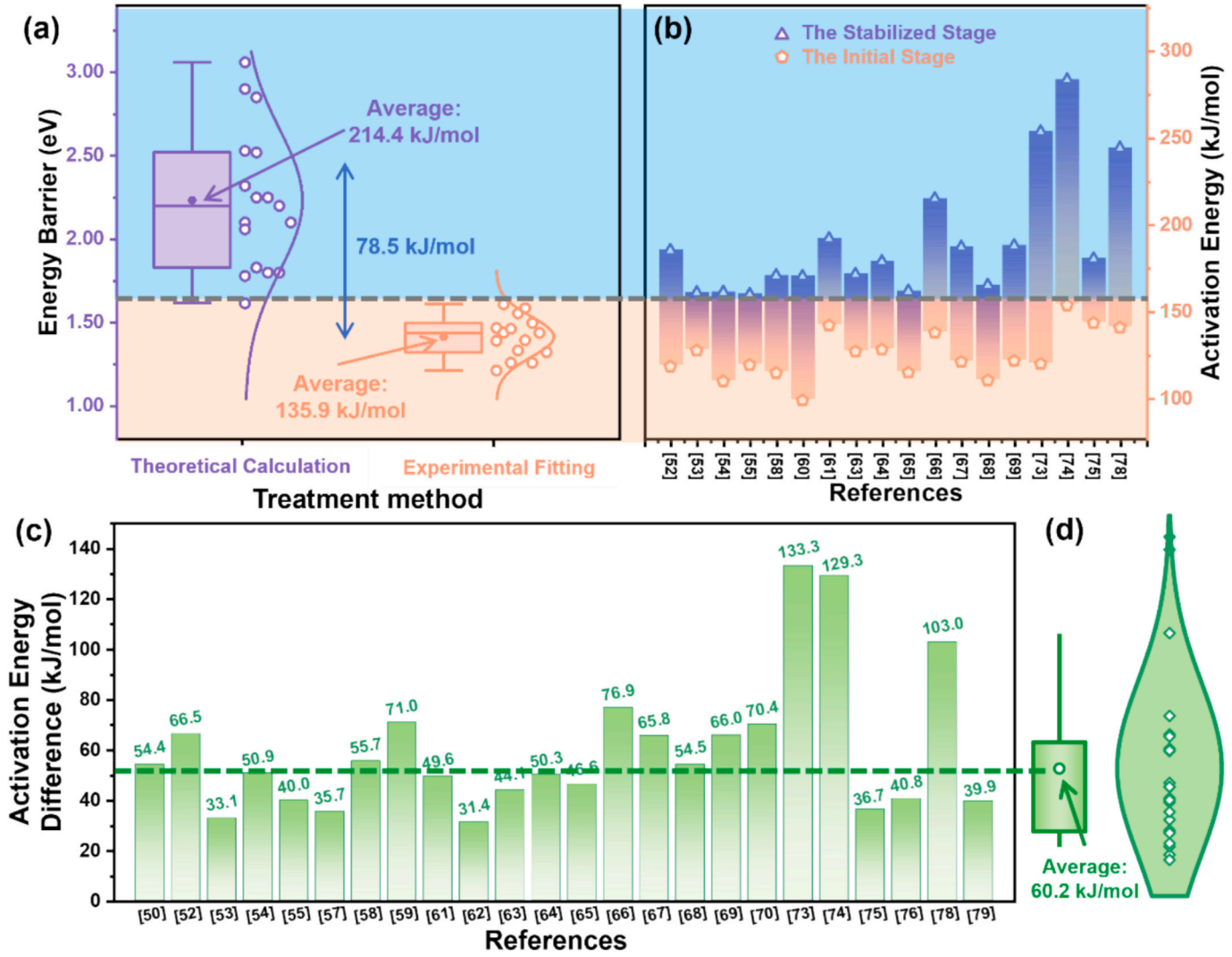

Fig. 4. (a) Statistical distributions of activation energies from theoretical calculations and experimental fittings. (b) Comparison of initial and equilibrium activation energies derived from the CEKP model. (c) Differences between initial and equilibrium activation energies based on CEKP analysis. (d) Violin plot of the activation energy differences.

suitable for comparison with the initial high-barrier region of the CEKP-derived activation energy profiles.

As shown in Fig. 4(a), the activation energy values obtained from literature using theoretical calculation and experimental fitting exhibit two distinct probability distributions. Most activation energy values derived from theoretical calculations exceed 155 kJ/mol, whereas those obtained from experimental fitting are often lower than this threshold. Theoretical values derived from density functional theory show an average of 214.4 kJ/mol. In contrast, experimental fitting yields an average of 135.9 kJ/mol. These data reflect a consistent numerical gap between the two methodologies. Fig. 4(b) presents the reported ranges of initial and equilibrium activation energies from representative studies. It can be observed that the initial activation energy in each case falls within the theoretical range, whereas the equilibrium values closely align with the experimental fitting range. This observation supports the conclusion that the discrepancy arises from their respective focus on different reaction stages, with the burst effect serving as the key factor responsible for the divergence. This observation supports the conclusion that the discrepancy arises from their respective focus on different reaction stages, with the burst effect serving as the key factor responsible for the divergence.

The results provide direct quantitative evidence that the CEKP model effectively captures the dynamic evolution of activation energy and bridges the gap between theoretical and experimental approaches. This agreement can be primarily attributed to the fundamental difference in spatial and temporal resolution between theoretical simulations and experimental kinetic fittings. Theoretical calculations typically operate on the atomic scale and within picosecond timescales due to computational limitations, and thus predominantly capture the initial surface desorption processes [88–93]. When simulations are extended to include multiple hydrogen-containing layers and longer timescales, the characteristic burst effect, characterized by a sharp drop in activation energy, begins to emerge [34]. In contrast, experimental fittings are based on macroscopic measurements over much longer durations, often emphasizing the steady-state regime of dehydrogenation and overlooking the high-barrier initial stage [94–97]. This intrinsic mismatch in kinetic observation windows is a major source of the apparent discrepancy in activation energy between simulations and experiments. Fig. 4(c) presents the energy difference between the initial and stabilized stages calculated from the CEKP model ranges from 31.4 to 133.3 kJ/mol, which is consistent with the range reported in both experimental and theoretical studies. Furthermore, Fig. 4(d) shows the statistical distribution of these energy differences in the form of a violin plot. The average difference between the initial and stabilized activation energies is calculated to be 60.2 kJ/mol, which closely matches the 78.5 kJ/mol average difference observed between theoretical and experimental results in Fig. 4(a). This numerical consistency further confirms the capability of the CEKP framework to provide a unified kinetic interpretation that accommodates both simulation and experimental perspectives, and demonstrates that the burst effect is not a computational artifact, but rather a physically meaningful transition embedded in the dehydrogenation pathway.

These findings provide a data-driven and physically interpretable explanation for the divergence between theoretical simulations and experimental fittings, and establish a unified kinetic perspective that encompasses both the early-stage surface processes and the later-stage bulk evolution. Rather than attempting to eliminate such differences, it is more meaningful to recognize and utilize the dynamic transition revealed by the burst effect. In this context, catalysts are expected not only to enhance reaction kinetics at the surface but also to effectively modulate the entire dehydrogenation pathway. By promoting the onset of the burst effect and facilitating subsequent bulk hydrogen diffusion, catalytic strategies can substantially improve the practical hydrogen release performance of magnesium-based materials. This insight offers valuable guidance for the rational design of next-generation solid-state hydrogen storage systems and their application in energy storage technologies [98]. For example, the identification of high activation energy in the initial stage suggests that efforts should be directed toward overcoming the early-stage kinetic barrier. Surface modification approaches such as nanosizing, catalyst doping, or the introduction of lattice defects may help lower the initial energy threshold, thereby triggering the burst effect earlier and enabling a more efficient overall dehydrogenation process.

4. Conclusion

This study proposes a dynamic kinetic modeling framework to systematically investigate the dehydrogenation process of magnesium hydride. Emphasis is placed on providing direct macroscopic evidence for the burst effect. By integrating a large volume of literature-reported kinetic data and utilizing a data-driven modeling approach based on the JMAK framework, the dynamic evolution of activation energy throughout the reaction process is reconstructed. The results reveal a consistent trend across various experimental conditions: an initial sharp decline in activation energy followed by stabilization, which offers reproducible evidence for the burst effect mechanism.

The continuity and statistical robustness of the constructed kinetic profiles bridge the long-standing discrepancy between theoretical calculations and experimental fittings. The proposed evolving activation energy function captures both the high-energy barrier associated with surface desorption and the subsequent diffusion-limited regime, providing a unified physical interpretation of the dehydrogenation process. This approach not only validates the burst effect with quantitative kinetic evidence but also reinterprets the divergence between theoretical and experimental activation energies from a dynamic perspective. Despite the demonstrated robustness of the continuously evolving kinetic parameter framework, localized deviations may still arise due to data segmentation and experimental uncertainties. Future research should incorporate high-accuracy theoretical calculations and real-time kinetic measurements to further refine the activation energy landscape and strengthen the physical foundation of the model.

Looking forward, the definitive validation of the burst effect provides not only a physical foundation for understanding the dehydrogenation behavior of magnesium hydride but also new possibilities for practical applications in the energy storage field. The two-stage kinetic feature, comprising an initial rapid hydrogen release followed by a stable diffusion-limited phase, offers measurable parameters for multiscale simulation, thermal management design, and precise dehydrogenation control. In engineering practice, strategies such as increasing the surface area or optimizing the interface structure may further amplify the kinetic advantages of the burst stage. Additionally, the proposed modeling approach can be generalized to other gas-solid systems, contributing to the identification and control of kinetic heterogeneity in complex reactions. Continued investigation of the burst effect will support the development of intelligent hydrogen storage systems and promote the integration of data-driven methodologies in solid-state reaction kinetics.

CRediT authorship contribution statement

Jianghao Cai: Writing – review & editing, Writing – original draft, Visualization, Methodology, Data curation. **Haobo Wang:** Investigation, Data curation. **Xiaotian Tang:** Writing – review & editing, Data curation. **Ziwei Miao:** Writing – review & editing. **Tongao Yao:** Investigation, Formal analysis. **Yuxuan Liu:** Visualization, Data curation. **Hongtao Wang:** Writing – review & editing. **Zhengyang Gao:** Supervision, Project administration. **Weijie Yang:** Writing – review & editing, Supervision, Funding acquisition.

Declaration of Generative AI and AI-assisted technologies in the writing process

During the preparation of this work, the authors used ChatGPT in

order to improve language expression and check grammar. After using this tool, the authors reviewed and edited the content as needed and take full responsibility for the content of the publication.

Declaration of competing interest

The authors declare that they have no known competing financial interests or personal relationships that could have appeared to influence the work reported in this paper.

Data availability

Data will be made available on request.

Acknowledgements

The authors gratefully acknowledge the Solid-State Hydrogen Storage Materials Digital Analysis Platform (https://s-hydrogendataplatform.nas.cpolar.cn/, Digital Hydrogen-S) for providing access to critical datasets that supported the statistical analysis conducted in this study.

This research was supported by the Natural Science Foundation of Hebei Province (E2023502006) and Fundamental Research Fund for the Central Universities (2025MS131).

Appendix A. Supplementary data

Supplementary data to this article can be found online at https://doi.org/10.1016/j.est.2025.118450.

References

[1] S. Zhou, W. Cao, L. Shang, et al., Facilitating alkaline hydrogen evolution kinetics via interfacial modulation of hydrogen-bond networks by porous amine cages, Nat. Commun. 16 (1) (2025).
[2] Q. Zhang, Y. Shan, J. Pan, et al., A photovoltaic-electrolysis system with high solar-to-hydrogen efficiency under practical current densities, Sci. Adv. 11 (9) (2025).
[3] J. Zheng, X. Liu, P. Xu, et al., Development of high pressure gaseous hydrogen storage technologies, Int. J. Hydrog. Energy 37 (1) (2012) 1048–1057.
[4] J. Wu, S. Chen, M. Yu, et al., Techno-economic analysis on low-temperature and high-pressure cryo-adsorption hydrogen storage, Fuel 381 (2025) 133532.
[5] H. Kim, H. Kim, W. Kim, et al., Facile synthesis of nanoporous Mg crystalline structure by organic solvent-based reduction for solid-state hydrogen storage, Nat. Commun. 15 (1) (2024).
[6] J. Cai, Y. Jiang, T. Yao, et al., A demand-driven dynamic heating strategy for ultrafast and energy-efficient MgH_2 dehydrogenation utilizing the “burst effect”, J. Energy Storage 130 (2025) 117495.
[7] X. Zhang, S. Ju, C. Li, et al., Atomic reconstruction for realizing stable solar-driven reversible hydrogen storage of magnesium hydride, Nat. Commun. 15 (1) (2024) 2815.
[8] S. Dong, H. Liu, X. Liu, et al., Facile dehydrogenation of MgH_2 enabled by γ-graphyne based single-atom catalyst, J. Energy Storage 74 (2023) 109484.
[9] L. Ren, Y. Li, N. Zhang, et al., Nanostructuring of Mg-based hydrogen storage materials: recent advances for promoting key applications, Nano-Micro Lett. 15 (1) (2023) 93.
[10] H. Yang, Z. Ding, Y. Li, et al., Recent advances in kinetic and thermodynamic regulation of magnesium hydride for hydrogen storage, Rare Metals 42 (9) (2023) 2906–2927.
[11] Z. Ding, Y. Li, H. Yang, et al., Tailoring MgH_2 for hydrogen storage through nanoengineering and catalysis, J. Magnes. Alloys 10 (2022) 2946–2967.
[12] H. Jiang, Z. Ding, Y. Li, et al., Hierarchical interface engineering for advanced magnesium-based hydrogen storage: synergistic effects of structural design and compositional modification, Chem. Sci. 16 (2025) 7610.
[13] H. Guan, Y. Lu, J. Liu, et al., Microscopic scaling relation of Ti-based catalysts in de/hydrogenation reactions of Mg/MgH_2, ACS Catal. 14 (2024) 17159–17170.
[14] D. Zhou, D. Zhao, H. Sun, et al., Two-dimensional material MXene and its derivatives enhance the hydrogen storage properties of MgH_2: A review and summary, Int. J. Hydrog. Energy 71 (2024) 279–297.
[15] H. Wang, J. Li, X. Wei, et al., Thermodynamic and kinetic regulation for Mg-based hydrogen storage materials: challenges, strategies, and perspectives, Adv. Funct. Mater. 34 (42) (2024) 2406639.
[16] N. Klopcic, I. Grimmer, F. Winkler, et al., A review on metal hydride materials for hydrogen storage, J. Energy Storage 72 (2023) 108456.
[17] Q. Li, X. Lin, Q. Luo, et al., Kinetics of the hydrogen absorption and desorption processes of hydrogen storage alloys: a review, Int. J. Miner. Metall. Mater. 29 (1) (2022) 32–48.
[18] Y. Pang, Q. Li, A review on kinetic models and corresponding analysis methods for hydrogen storage materials, Int. J. Hydrog. Energy 41 (40) (2016) 18072–18087.
[19] R. Wang, Z. Liu, L. Ji, et al., Reaction kinetics of CaC_2 formation from powder and compressed feeds, Front. Chem. Sci. Eng. 10 (4) (2016) 517–525.
[20] S. Ma, F. Xing, N. Ta, et al., Kinetic modeling of high-temperature oxidation of pure Mg, J. Magnes. Alloys 8 (3) (2020) 819–831.
[21] A. Neves, J. Puszkiel, G. Capurso, et al., Development of a new approach for the kinetic modeling of the lithium reactive hydride composite (Li-RHC) for hydrogen storage under desorption conditions, Chem. Eng. J. 464 (2023) 142274.
[22] D. Bhattacharjya, T. Selvamani, I. Mukhopadhyay, Thermal decomposition of hydromagnesite, J. Therm. Anal. Calorim. 107 (2) (2012) 439–445.
[23] R. Campostrini, M. Abdellatief, M. Leoni, et al., Activation energy in the thermal decomposition of MgH_2 powders by coupled TG-MS measurements, J. Therm. Anal. Calorim. 116 (1) (2014) 225–240.
[24] M. Avrami, Kinetics of phase change. I general theory, J. Chem. Phys. 7 (12) (1939) 1103–1112.
[25] T. Huang, H. Liu, C. Zhou, Effect of driving force on the activation energies for dehydrogenation and hydrogenation of catalyzed MgH_2, Int. J. Hydrog. Energy 46 (76) (2021) 37986–37994.
[26] C. Yan, X. Lu, J. Zheng, et al., Dual-cation K_2TaF_7 catalyst improves high-capacity hydrogen storage behavior of MgH_2, Int. J. Hydrog. Energy 48 (15) (2023) 6023–6033.
[27] Q. Luo, J. Li, B. Li, et al., Kinetics in Mg-based hydrogen storage materials: Enhancement and mechanism, J. Magnes. Alloys 7 (1) (2019) 58–71.
[28] Y. Pang, D. Sun, Q. Gu, et al., Comprehensive determination of kinetic parameters in solid-state phase transitions: an extended Jonhson-Mehl-Avrami-Kolomogorov model with analytical solutions, Cryst. Growth Des. 16 (4) (2016) 2404–2415.
[29] T. Huang, C. Zhou, Surface diffusion-controlled Jonhson-Mehl-Avrami-Kolmogorov model for hydrogenation of Mg-based alloys, J. Phys. Chem. C 127 (28) (2023) 13900–13910.
[30] A. Kempen, F. Sommer, E. Mittemeijer, Determination and interpretation of isothermal and non-isothermal transformation kinetics; the effective activation energies in terms of nucleation and growth, J. Mater. Sci. 37 (7) (2002) 1321–1332.
[31] J. Kapischke, J. Hapke, Measurement of the effective thermal conductivity of a Mg-MgH_2 packed bed with oscillating heating, Exp. Thermal Fluid Sci. 17 (4) (1998) 347–355.
[32] C. Zhou, C. Hu, Y. Li, et al., Crystallite growth characteristics of Mg during hydrogen desorption of MgH_2, Prog. Nat. Sci. Mater. Int. 30 (2) (2020) 246–250.
[33] J. Karst, F. Sterl, H. Linnenbank, et al., Watching in situ the hydrogen diffusion dynamics in magnesium on the nanoscale, Sci. Adv. 6 (19) (2020) eaaz0566.
[34] S. Dong, C. Li, J. Wang, et al., The “burst effect” of hydrogen desorption in MgH_2 dehydrogenation, J. Mater. Chem. A 10 (42) (2022) 22363–22372.
[35] C. Li, W. Yang, H. Liu, et al., Picturing the gap between the performance and US-DOE’s hydrogen storage target: A data-driven model for MgH_2 dehydrogenation, Angew. Chem. Int. Ed. Eng. 63 (28) (2024) e202320151.
[36] J. Ma, J. Liu, X. Jiang, et al., A two-dimensional distributed activation energy model for pyrolysis of solid fuels, Energy 230 (2021) 120860.
[37] A. Soria, M. Rubio, E. Goos, et al., Combining the lumped capacitance method and the simplified distributed activation energy model to describe the pyrolysis of thermally small biomass particles, Energy Convers. Manag. 175 (2018) 164–172.
[38] S. Wakimoto, Y. Matsukawa, Y. Numazawa, et al., Neural network estimation of kinetic parameters in distributed activation energy model (DAEM) without a priori assumptions for parallel reaction system, Fuel 343 (2023) 127836.
[39] W. Zhang, Y. Zhang, H. Wu, et al., Investigation on the pyrolysis behaviors and kinetics of walnut shell lignocellulosic biomass with additives, Chin. J. Chem. Eng. 80 (2025) 303–314.
[40] S. Quan, Y. Zeng, Y. Wu, et al., Ash thermomechanical properties and combustion characteristics during Co-combustion of anthracite and biomass for CFB combustors, Biomass Bioenergy 198 (2025) 107868.
[41] J. Hristov, A note on the Johnson-Mehl-Avrami-Kolmogorov kinetic model: an attempt aiming to introduce time non-locality, Eng 6 (2) (2025) 24.
[42] O. Pedroso, Y. Champion, W. Botta, et al., Johnson-Mehl-Avrami-Kolmogorov model applied to describe the site blocking effect in interstitial solid solution, Acta Mater. 271 (2024) 119907.
[43] R. Svoboda, Crystallization of glasses-when to use the Johnson-Mehl-Avrami kinetics? J. Eur. Ceram. Soc. 41 (15) (2021) 7862–7867.
[44] O. Bylya, A. Reshetov, N. Stefani, et al., Applicability of JMAK-type model for predicting microstructural evolution in nickel-based superalloys, Procedia Eng. 207 (2017) 1105–1110.
[45] X. Lin, Q. Zhu, H. Leng, et al., Numerical analysis of the effects of particle radius and porosity on hydrogen absorption performances in metal hydride tank, Appl. Energy 250 (2019) 1065–1072.
[46] H. Liu, X. Duan, Z. Wu, et al., Exfoliation of compact layered Ti_2VAlC_2 MAX to open layered Ti_2VC_2 MXene towards enhancing the hydrogen storage properties of MgH_2, Chem. Eng. J. 468 (2023) 143688.
[47] F. Yin, Z. Chen, T. Si, et al., Structural-regulation of Laves phase high-entropy alloys to catalytically enhance hydrogen desorption from MgH_2, J. Alloys Compd. 997 (2024) 174822.
[48] A. Watpade, S. Thakor, P. Jain, et al., Comparative analysis of machine learning models for predicting dielectric properties in MoS_2 nanofiller-reinforced epoxy composites, Ain Shams Eng. J. 15 (6) (2024) 102754.
[49] R. Ramprasad, R. Batra, G. Pilania, et al., Machine learning in materials informatics: recent applications and prospects, npj Comput. Mater. 3 (1) (2017) 54.

[50] D. Tan, C. Peng, Q. Zhang, Microstructural characteristics and hydrogen storage properties of the Mg-Ni-TiS_2 nanocomposite prepared by a solution-based method, Int. J. Hydrog. Energy 48 (44) (2023) 16756–16768.
[51] S. Wu, Y. Chen, W. Kang, et al., Hydrogen storage properties of MgTiVZrNb high-entropy alloy and its catalytic effect upon hydrogen storage in Mg, Int. J. Hydrog. Energy 50 (2024) 1113–1128.
[52] J. Wu, Z. Liu, H. Zhang, et al., Hydrogen storage performance of MgH_2 under catalysis by highly dispersed nickel-nanoparticle-doped hollow spherical vanadium nitride, J. Magnes. Alloys 12 (12) (2024) 5132–5143.
[53] Z. Lan, H. Liang, X. Wen, et al., Experimental and theoretical studies on two-dimensional vanadium carbide hybrid nanomaterials derived from V_4AlC_3 as excellent catalyst for MgH_2, J. Magnes. Alloys 11 (10) (2023) 3790–3799.
[54] Z. Liu, H. Ning, R. Liu, et al., Fabrication of V_2O_3-TiO_2-rGO ternary heterojunction composite to enhance the hydrogen storage performance of MgH_2, Chem. Eng. J. 499 (2024) 155877.
[55] J. Zhang, C. Zheng, Y. Wang, et al., Effect of La-Ni@$_3$DG catalyst concentration on the hydrogen storage properties of MgH_2, Int. J. Hydrog. Energy 95 (2024) 666–677.
[56] S. Ding, Y. Qiao, X. Cai, et al., A novel carbon-induced-porosity mechanism for improved cycling stability of magnesium hydride, J. Magnes. Alloys 13 (3) (2025) 1341–1352.
[57] H. Wan, X. Yang, S. Zhou, et al., Enhancing hydrogen storage properties of MgH_2 using FeCoNiCrMn high entropy alloy catalysts, J. Mater. Sci. Technol. 149 (2023) 88–98.
[58] X. Lu, L. Zhang, H. Yu, et al., Achieving superior hydrogen storage properties of MgH_2 by the effect of TiFe and carbon nanotubes, Chem. Eng. J. 422 (2021) 130101.
[59] D. Khan, J. Zou, S. Panda, et al., Mechanism of thermodynamic destabilization and fast desorption kinetics in a mechanically alloyed MgH_2-in composite, J. Phys. Chem. C 124 (18) (2020) 9685–9695.
[60] C. Lu, Y. Ma, F. Li, et al., Visualization of fast "hydrogen pump" in core-shell nanostructured Mg@Pt through hydrogen-stabilized Mg_3Pt, J. Mater. Chem. A 7 (24) (2019) 14629–14637.
[61] L. Zhang, X. Lu, L. Ji, et al., Catalytic effect of facile synthesized $TiH_{1.971}$ nanoparticles on the hydrogen storage properties of MgH_2, Nanomaterials 9 (10) (2019) 1370.
[62] L. Zhang, X. Lu, Z. Sun, et al., Superior catalytic effect of facile synthesized $LaNi_{4.5}Mn_{0.5}$ submicro-particles on the hydrogen storage properties of MgH_2, J. Alloys Compd. 844 (2020) 156069.
[63] T. Zhong, T. Xu, L. Zhang, et al., Designing multivalent NiMn-based layered nanosheets with high specific surface area and abundant active sites for solid-state hydrogen storage in magnesium hydride, J. Magnes. Alloys 13 (1) (2025) 148–160.
[64] X. Ou, J. Li, H. Lv, et al., Effect of nanosized nickel diselenide on hydrogen storage properties of ball-milled magnesium hydride, Int. J. Hydrog. Energy 101 (2025) 594–604.
[65] Y. Chen, B. Sun, G. Zhang, et al., MOF-derived Ni_3Fe/Ni/$NiFe_2O_4$@C for enhanced hydrogen storage performance of MgH_2, J. Energy Chem. 101 (2025) 333–344.
[66] S. Zhao, T. Wu, K. Wang, et al., Synergistic dual-modification regulation of dehydrogenation kinetics of MgH_2 by MOF-derived Core-shell Ni&C, Int. J. Hydrog. Energy 127 (2025) 241–251.
[67] L. Wang, L. Zhang, F. Wu, et al., Promoting catalysis in magnesium hydride for solid-state hydrogen storage through manipulating the elements of high entropy oxides, J. Magnes. Alloys 12 (12) (2024) 5038–5050.
[68] Z. Tian, Z. Wang, P. Yao, et al., Hydrogen storage behaviors of magnesium hydride catalyzed by transition metal carbides, Int. J. Hydrog. Energy 46 (80) (2021) 40203–40216.
[69] X. Huang, C. Lu, Y. Li, et al., Hydrogen release and uptake of MgH_2 modified by Ti_3CN MXene, Inorganics 11 (6) (2023) 243.
[70] C. Zhu, T. Akiyama, Zebra-striped fibers in relation to the H_2 sorption properties for MgH_2 nanofibers produced by a vapor-solid process, Cryst. Growth Des. 12 (8) (2012) 4043–4052.
[71] Z. Lu, H. Yu, X. Lu, et al., Two-dimensional vanadium nanosheets as a remarkably effective catalyst for hydrogen storage in MgH_2, Rare Metals 40 (11) (2021) 3195–3204.
[72] T. Tian, X. Wang, K. Shi, et al., Boosting hydrogen storage performance of MgH_2 by efficient V_2O_3/C catalyst, J. Alloys Compd. 1010 (2025) 178333.
[73] S. Li, L. Zhang, F. Wu, et al., Efficient catalysis of FeNiCu-based multi-site alloys on magnesium-hydride for solid-state hydrogen storage, Chin. Chem. Lett. 36 (1) (2025) 109566.
[74] D. Gao, F. Wu, Z. Zhang, et al., Graphene-loaded nickel-vanadium bimetal oxides as hydrogen pumps to boost solid-state hydrogen storage kinetic performance of magnesium hydride, Trans. Nonferrous Metals Soc. China 34 (8) (2024) 2645–2657.
[75] Y. Chen, B. Sun, G. Zhang, et al., Catalytic effect of double transition metal sulfide NiCo2S4 on hydrogen storage properties of MgH_2, Appl. Surf. Sci. 645 (2024) 158801.
[76] B. Zhang, X. Xie, Y. Wang, et al., In situ formation of multiple catalysts for enhancing the hydrogen storage of MgH_2 by adding porous $Ni_3ZnC_{0.7}$/Ni loaded carbon nanotubes microspheres, J. Magnes. Alloys 12 (3) (2024) 1227–1238.
[77] C. Lu, H. Liu, L. Xu, et al., Two-dimensional vanadium carbide for simultaneously tailoring the hydrogen sorption thermodynamics and kinetics of magnesium hydride, J. Magnes. Alloys 10 (4) (2022) 1051–1065.
[78] Y. Jiang, N. Si, W. Jiang, et al., FeNiCu-based composite catalyst for hydrogen storage in MgH_2, Chem. Eng. J. 499 (2024) 156449.
[79] M. Song, F. Wu, Y. Jiang, et al., Optimizing FeCoNiCrTi high-entropy alloy with hydrogen pumping effect to boost de/hydrogenation performance of magnesium hydride, Rare Metals 43 (7) (2024) 3273–3285.
[80] W. Fu, M. Shu, X. Liu, et al., Unveiling the micro-mechanism of superior dehydrogenation in γ-MgH_2: Insights into electronic structure of H-Mg bond, J. Alloys Compd. 1306 (2025) 182130.
[81] A. Du, S. Smith, X. Yao, et al., Ab initio studies of hydrogen desorption from low index magnesium hydride surface, Surf. Sci. 600 (9) (2006) 1854–1859.
[82] G. Wu, J. Zhang, Q. Li, et al., Dehydrogenation kinetics of magnesium hydride investigated by DFT and experiment, Comput. Mater. Sci. 49 (1) (2010) S144–S149.
[83] L. Wang, D. Johnson, Hydrogen desorption from Ti-doped MgH_2(110) surfaces: catalytic effect on reaction pathways and kinetic barriers, J. Phys. Chem. C 116 (14) (2012) 7874–7878.
[84] S. Maintz, V. Deringer, A. Tchougréeff, et al., Analytic projection from plane-wave and PAW wavefunctions and application to chemical-bonding analysis in solids, J. Comput. Chem. 34 (29) (2013) 2557–2567.
[85] H. Wang, D. Wu, L. Wei, et al., First-principles investigation of dehydrogenation on cu-doped MgH_2 (001) and (110) surfaces, J. Phys. Chem. C 118 (25) (2014) 13607–13616.
[86] H. Chen, H. Yu, Q. Zhang, et al., Enhancement in dehydriding performance of magnesium hydride by iron incorporation: a combined experimental and theoretical investigation, J. Power Sources 322 (2016) 179–186.
[87] A. Oliveira, A. Pavão, Theoretical study of hydrogen storage in metal hydrides, J. Mol. Model. 24 (6) (2018) 127.
[88] X. Xie, C. Hou, C. Chen, et al., First-principles studies in Mg-based hydrogen storage materials: a review, Energy 211 (2020) 118959.
[89] S. Dong, C. Li, E. Lv, et al., MgH_2/single-atom heterojunctions: effective hydrogen storage materials with facile dehydrogenation, J. Mater. Chem. A 10 (37) (2022) 19839–19851.
[90] Y. Fu, Z. Yu, S. Guo, et al., Catalytic effect of bamboo-like carbon nanotubes loaded with NiFe nanoparticles on hydrogen storage properties of MgH_2, Chem. Eng. J. 458 (2023) 141337.
[91] J. Chen, Z. Wang, Z. Meng, et al., The effects and mechanisms of two-dimensional V_2C and V_2CT_2 (t = O, F, and OH) on hydrogen adsorption and dissociation properties of MgH_2: first-principles calculations, Int. J. Hydrog. Energy 87 (2024) 1180–1188.
[92] Y. Huang, J. Chang, Q. Tian, et al., Heteroatom sulfur exploration for enhancing MgH_2 dehydrogenation: A theoretical and experimental analysis, Int. J. Hydrog. Energy 68 (2024) 51–62.
[93] H. Han, W. Jiang, N. Si, et al., Catalytic effect of Si_2BN monolayer on the dehydrogenation of MgH_2: first-principles study, Int. J. Hydrog. Energy 109 (2025) 497–505.
[94] L. Zhang, F. Nyahuma, H. Zhang, et al., Metal organic framework supported niobium pentoxide nanoparticles with exceptional catalytic effect on hydrogen storage behavior of MgH_2, Green Energy Environ. 8 (2) (2023) 589–600.
[95] N. Sulaiman, N. Juahir, N. Mustafa, et al., Improved hydrogen storage properties of MgH_2 catalyzed with K_2NiF_6, J. Energy Chem. 25 (5) (2016) 832–839.
[96] N. Sazelee, N. Idris, M. Md, et al., Synthesis of $BaFe_{12}O_{19}$ by solid state method and its effect on hydrogen storage properties of MgH_2, Int. J. Hydrog. Energy 43 (45) (2018) 20853–20860.
[97] N. Mustafa, M. Ismail, Hydrogen sorption improvement of MgH_2 catalyzed by CeO_2 nanopowder, J. Alloys Compd. 695 (2017) 2532–2538.
[98] L. Xuao, L. Shiwen, L. Jiongyang, et al., FIND: a forward–inverse navigation and discovery platform for hydrogen storage alloys powered by data-driven machine learning, J. Mater. Inf. 5 (2025) 48.